Journal of Alloys and Compounds 509 (2011) 1452–1456

Contents lists available at ScienceDirect

Journal of Alloys and Compounds

journal homepage: www.elsevier.com/locate/jallcom

Spectroscopic and crystal field analysis of absorption and photoluminescence properties of red phosphor $CaAl_{12}O_{19}:Mn^{4+}$ modified by MgO

M.G. Brik[a,*], Y.X. Pan[b,c], G.K. Liu[b]

[a] Institute of Physics, University of Tartu, Riia 142, Tartu 51014, Estonia
[b] Chemical Sciences and Engineering Division, Argonne National Laboratory, Argonne, IL 60439, USA
[c] Nanomaterials and Chemistry Key Laboratory, Wenzhou University, Wenzhou 325027, PR China

ARTICLE INFO

Article history:
Received 26 October 2010
Received in revised form
11 November 2010
Accepted 17 November 2010
Available online 23 November 2010

Keywords:
Photoluminescence
Red phosphor
Crystal field modeling

ABSTRACT

The spectroscopic properties of a series of red phosphors with general composition of $CaAl_{12}O_{19}:yMn^{4+}$ and $(Ca_{1-x}Al_{12}O_{19}, xMgO):yMn^{4+}$ ($x = 0–1$, $y = 0.001–1.5\%$) synthesized by a modified solid state method in air have been investigated in detail. Addition of MgO is necessary for Mn^{4+} charge compensation and leads to the formation of separate crystal phases of Al_2O_3 and $MgAl_2O_4$, which was confirmed by the XRD studies. Enhancement of Mn^{4+} luminescence with increasing content of MgO was observed and a mechanism for explanation of this phenomenon is suggested. For an analysis of the crystal phases and luminescent efficiency of the phosphors in the prepared series, crystal field calculations of the Mn^{4+} energy levels have been performed. This theoretical approach allowed for assigning the observed excitation and emission spectra. Red shift of the Mn^{4+} luminescence with increasing concentration of Mg ions is explained from the point of view of enhanced nephelauxetic effect after doping.

1. Introduction

Fabrication of blue GaN LEDs with yellow garnet phosphor is one of the most common technologies for currently used solid-state lighting [1–3]. For the next generation of lighting products, targeting white LEDs are expected to reproduce the sunlight spectrum accurately. However, it should be noted that the current two-color white LEDs fabricated with YAG:Ce are not able to get enough high color rendering due to deficiency of red color in the phosphors' luminescence spectra. Various methods such as co-doping with additional rare earth activators (to increase red components of emission bands by red shift of emission bands of the garnet phosphors through changing crystal lattices) have been employed so far for improvement of the garnet phosphors' performance. However, the modified garnet derivatives show better emission power distribution in red but come at the expense of energy efficiency [4–7]. Therefore, for a white light LED with higher color rendering and high efficiency, it is feasible to mix a high efficient red phosphor into YAG:Ce. We also note that $SrTiO_3:Pr^{3+}$ co-doped with Mg and Zn has been reported recently to be a promising red phosphor [8].

The family of phosphors doped with Eu^{3+} ions are the common components for conventional lighting due to their high efficiencies and color purities, but the sharp absorption peaks originated from the Eu^{3+} f–f transitions in UV and blue region limit their application in current white LEDs [9,10]. A red phosphor Mn^{4+}-doped $3.5MgO{\cdot}0.5MF_2{\cdot}GeO_2$ (MFGO:Mn) is currently commercially used for improvement of the color rendering of the fluorescent lamps. However, its applications are also limited to very special cases due to a high price of GeO_2 [11]. Mn^{4+} doped $CaAl_{12}O_{19}$ (CAO), based on the d–d transitions of manganese ion within its $3d^3$ electron configuration, is an identified red phosphor with broad absorption band in visible region and superior chromaticity in deep red region [12,13]. It has been reported that the luminescent intensity of Mn^{4+} doped CAO phosphor could be enhanced by mixing CaF_2 as flux and MgF_2 for charge compensation [13]. However, for successful application in current white LEDs, its luminescent efficiency still needs to be further improved.

As recently reported, a remarkable enhancement of the luminescent efficiency of the $CaAl_{12}O_{19}:Mn^{4+}$ (CAO:Mn) phosphor has been achieved by composition modification through mixing with MgO [14]. Transformation of Mn^{4+} ion-pairs to isolated Mn^{4+} ions with charge compensation provided by Mg^{2+} is presumably the leading mechanism responsible for the luminescence enhancement. It is expected that the phosphors' composition modifications described in this work could be applied effectively to other similar phosphor systems to prevent ion-pair formation and/or make charge compensation, thereby improve their luminescent efficiencies. A fundamental understanding of the electronic energy level structure and its dependence on lattice environment is essential for further improving phosphor performance and development of new phosphors. With this aim in view, in addition to detailed spectroscopic and XRD measurements of properties of pure and Mg-containing

* Corresponding author.
E-mail address: brik@fi.tartu.ee (M.G. Brik).

0925-8388/$ – see front matter © 2010 Elsevier B.V. All rights reserved.
doi:10.1016/j.jallcom.2010.11.117

CAO:Mn phosphor, we report here the results of crystal field calculations of the Mn^{4+} energy levels in CAO, which allowed us to assign absorption peaks of Mn^{4+} and estimate the values of the Racah parameters, best of all describing the Mn^{4+} energy levels. Crystal field calculations, which are performed for the first time for the title system, confirm the dominantly trigonal symmetry of the Mn^{4+} position, evidenced from the structure of the crystal field Hamiltonian and character of splitting of the orbitally degenerated states of Mn^{4+} ion. The observed above-mentioned red shift of the manganese luminescence with addition of Mg ions is explained by decrease of the Mn^{4+} ion Racah's parameters after doping (i.e. enhanced nephelauxetic effect).

In the following sections we describe the samples preparation, spectroscopic measurements and crystal filed calculations. The paper is concluded with a short summary.

2. Experimental

The phosphors with general composition of $(Ca_{1-x}Al_{12}O_{19}, Mg_xO):yMn^{4+}$ ($x = 0$, 0.2, 0.4, 0.5, 0.6, 0.8, 1 and $y = 0.0001$–1.5%) were synthesized by a modified solid-state reaction. Stoichiometric soluble metal salts $Ca(CH_3COO)_2{\cdot}H_2O$, $Mg(NO_3)_2$, $Al(NO_3)_3{\cdot}9H_2O$ and $Mn(CH_3COO)_2{\cdot}4H_2O$ (all chemicals were of 99.9% purity; obtained from Aldrich) were dissolved in ion-free water and mixed homogeneously at molecular-level under continuous stirring. The mixtures were heated continuously on a hot plate until crispy brown precursor powders were formed. The precursor powders were sintered at 1000 °C for 12 h and followed at 1500 °C for 3 h in air. Repeated grindings were performed between two sintering processes.

The XRD data were collected on a Scintag diffractometer using Cu Kα radiation. For luminescence measurements, a xenon lamp dispersed by a SPEX grating monochromator was used as an excitation source. The low temperature luminescence measurements were performed with samples in a liquid helium cryostat. For recording the time-resolved luminescent spectra, a pulsed (5 ns) Nd-YAG laser at 355 nm was used to pump the samples.

3. Experimental results and discussion

Though the starting materials are soluble metal salts and are mixed at molecular level, the crystallized CAO phase cannot be obtained until the sintering temperature is increased to 1500 °C. The XRD patterns in Fig. 1 show that the pure hexagonal CAO phase with space group of $P6_3/mmc$ (194) matching well with the standard data (JCPDS card No. 38-0470) is achieved without mixing with MgO. New diffraction peaks attributed to the phases of hexagonal Al_2O_3 (JCPD No. 43-1484) and cubic spinel $MgAl_2O_4$ (JCPD No. 21-1152) emerge in the samples with added MgO. When molecular ratio Ca^{2+}/Mg^{2+} is smaller than 1/4, the mixture of Al_2O_3 and $MgAl_2O_4$ predominates in the samples, although some traces of the CAO phase can be also identified. The CAO phase is absent in the sample when all of the Ca^{2+} ions were replaced by Mg^{2+} ions. Stoichiometric doping with Mn^{4+} has a negligible influence on the resultant crystal phases and structures. Characterized by XRD as shown in Fig. 1, the powder samples are crystalline particles of micrometer size; nanocrystallites were not evident.

The normalized excitation and corresponding emission spectra of phosphor CAO:Mn prepared in this work and the red phosphor MFGO:Mn excited by xenon light source at room temperature are shown in Fig. 2 for comparison. The broad excitation bands on the left are attributed to the transition from the $^4A_2$ ground state to the $^4T_2$ excited state of Mn^{4+} ions. As illustrated by the Tanabe–Sugano diagram (insert), the energy gap between the $^4A_2$ and $^4T_2$ states (both arising from the ^4F ground term) becomes widen with increasing crystal field. The red shift of excitation band from MFGO:Mn to CAO:Mn is attributed to the lower crystal field in CAO. The maxima at 416 nm and 466 nm suggest that the MFGO:Mn and CAO:Mn phosphors can be excited by near UV (23,800–26,300 cm^{-1}) and blue (21,000–23,000 cm^{-1}) LED light, respectively. It should be noted that the excitation spectra in this work have been rectified by a factor associated with the response

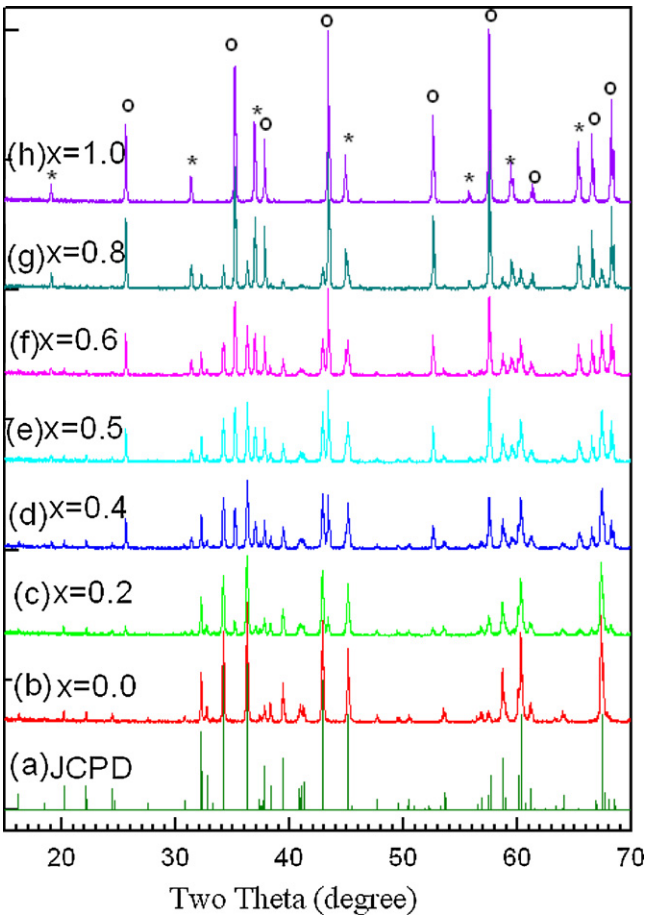

Fig. 1. (a) The standard XRD data of hexagonal $CaAl_{12}O_{19}$ in JCPD (#38-0470) and (b–h) XRD patterns of the phosphors $Ca_{1-x}Mg_xAl_{12}O_{19}:Mn^{4+}$ as a function of x. The empty spheres and stars mark the lines of Al_2O_3 and $MgAl_2O_4$ phases, respectively.

of measurement systems and intensity distribution of xenon lamp. The fine structure in the excitation spectrum of CAO:Mn reported in the literature may originate from xenon source [13]. The emission spectrum of MFGO:Mn shows typical 6 emission peaks in the

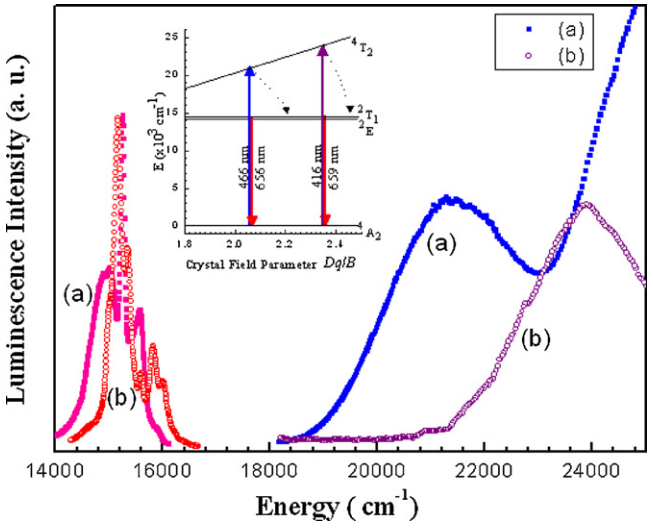

Fig. 2. Normalized emission (left) and excitation (right) spectra of phosphors (a) $CaAl_{12}O_{19}:0.5\%Mn^{4+}$ ($\lambda_{em} = 656$ nm, $\lambda_{ex} = 466$ nm), and (b) $3.5MgO{\cdot}0.5MgF_2{\cdot}GeO_2:1\%Mn^{4+}$ ($\lambda_{em} = 659$ nm, $\lambda_{ex} = 416$ nm) with xenon light source at room temperature. Insert: Tanabe–Sugano's diagram of Mn^{4+} (3d3) ion.

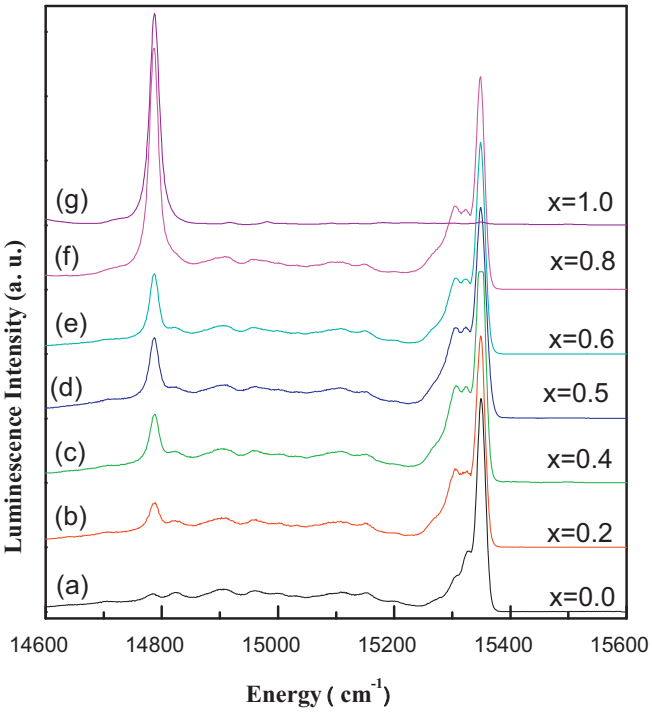

Fig. 3. Normalized emission spectra of phosphors $Ca_{1-x}Mg_xAl_{12}O_{19}:Mn^{4+}$ with x varying from 0.0 to 1.0 at 4.2 K.

region from 14,700 cm^{-1} to 16,100 cm^{-1} and the spectral feature is in accordance with the results reported previously [11]. The emission of CAO:Mn is located almost at the same wavelength as that of MFGO:Mn, which is due to the fact that the ^2E energy level of Mn^{4+} is almost independent of the crystal field. In this system, the position of the $^2T_1$ level (the next level to the ^2E state) is not identified, though its hot bands may also contribute to the main peak in emission spectra.

The emission spectra of the CAO:Mn phosphor excited at 460 nm at liquid helium temperature are exhibited in Fig. 3. The emission band in the region of 15,400–16,100 cm^{-1} is likely due to anti-Stokes vibronic sidebands associated with the ^2E excited state of Mn^{4+} ions, which disappears at 4 K. The strong emission peak part between 15,100 and 15,400 cm^{-1} is identified as the spin-forbidden ^2E–$^4A_2$ transition of Mn^{4+} ions, which has a blue shift at low temperature due to stronger crystal field splitting. The broad band in the region of 14,000–15,200 cm^{-1} is due to vibronic transitions of Mn^{4+} ions, which is much weaker at liquid helium temperature.

A new peak emerges at 14,750 cm^{-1} in low temperature emission spectra of the samples with MgO mixing in Fig. 3, which is not observed in the emission spectrum of Mn^{4+} in the pure phase of CAO. This is a clear manifestation that Mn^{4+} ions are in a phase, different from that of CAO. As we have seen in XRD patterns, two new phases Al_2O_3 and $MgAl_2O_4$ appear as the ratio of Mg/Ca increases. Based on the previous studies, no evidence of Mn^{4+} ions in the $MgAl_2O_4$ phase was observed [15,16]. It suggests that the emission peak at 14,750 cm^{-1} is attributed to the ^2E–$^4A_2$ transition of Mn^{4+} ions in Al_2O_3. The vibronic band for Mn^{4+} in the Al_2O_3 spread up to 13,890 cm^{-1} and overlap with a part of the vibronic transitions of Mn^{4+} in the CAO phase, which also contributes to the integrated intensity of the red luminescence band. Correspondingly, a new emission peak at 14,750 cm^{-1} grows up linearly with increasing Mg/Ca ratio in normalized emission spectra measured at 4 K. The peak at 14,750 cm^{-1} is not observed in the sample of CAO without MgO and the peak located 15,360 cm^{-1} disappears in the sample without Ca ions, which agrees well with the corresponding results indicated in XRD.

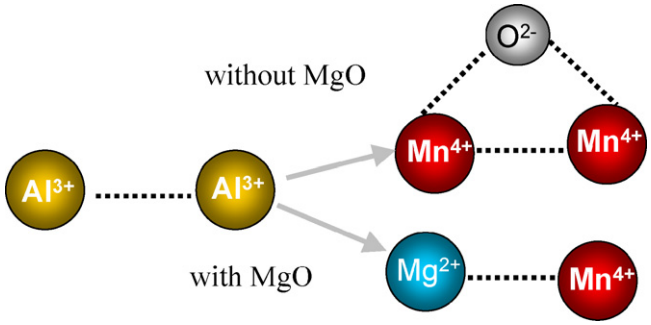

Fig. 4. Two mechanisms of charge compensation in CAO:Mn^{4+} without MgO (top) and with MgO (bottom). For simplicity, oxygen ions located between the Mn^{4+}–Mn^{4+} and Mg^{2+}–Mn^{4+} pairs are not shown.

A special attention should be paid to the role played by Mg ions in modifications of the luminescence properties of the prepared phosphors. It has been shown previously that the Cr^{3+} ions with incorporation into crystals as impurity ions tend to form pairs, when the concentration of Cr^{3+} exceeds 1% [17–19]. Since electronic structure and optical characteristic of Mn^{4+} ions are similar to those of isoelectronic Cr^{3+} ions, it is a reasonable assumption that Mn^{4+} ions are also inclined to form pairs in the CAO lattice to realize the charge compensation as illustrated in Fig. 4. Mn^{4+} ions may form pairs by trapping an interstitial O^{2-} ions and replace a couple of neighboring Al^{3+} ions for charge balance. The trend of forming the Mn^{4+}–Mn^{4+} pairs in combination with O^{2-} ions would be enhanced with increasing Mn^{4+} concentration. It will, therefore, significantly influence the excited state dynamics and reduce the luminescent efficiency of Mn^{4+} ions. When MgO is added, Mg^{2+} tends to occupy the Al^{3+} site in the CAO lattice, thus forming the Mn^{4+}–Mg^{2+} pairs. In this case, the charge compensation is achieved without involving any additional oxygen ions. As a result, the radiative transition probability of Mn^{4+} in the excited state will increase, which enhances the Mn^{4+} emission. Since two different phases (Al_2O_3 and $MgAl_2O_4$) were shown to co-exist and even dominate in the prepared samples with high content of MgO, a large part of Mg^{2+} ions does not enter the CAO lattice. However, for low concentrations of Mn^{4+} and small additions of MgO, some of Mg^{2+} ions tend to form Mn^{4+}–Mg^{2+} pairs to maintain properly the charge balance. This point of view is confirmed by the XRD diagrams in Fig. 1, where the characteristic CAO structure peaks are clearly seen in the samples with added MgO and disappear completely only when all Ca ions are replaced by Mg ions.

4. Crystal field calculations

$CaAl_{12}O_{19}$ crystals have hexagonal crystal structure, space group $P63/mmc$, with lattice constants (in Å) $a = 5.5587$ and $b = 21.8929$, angle $\gamma = 120^\circ$ [20]; one unit cell contains two formula units. After doping, Mn^{4+} ions substitute for Al^{3+} ions at the centers of slightly deformed octahedrons made by six oxygen ions. Fig. 5 shows the room-temperature extended excitation and luminescence spectra of $CaAl_{12}O_{19}:Mn^{4+}$ (0.5% of Mn ions).

Three main bands determine the overall appearance of the excitation spectrum; they are centered at about 466 nm (~21,460 cm^{-1}), 394 nm (~25,380 cm^{-1}) and 340 nm (~29,410 cm^{-1}). The first band can be unambiguously assigned to the spin-allowed $^4A_2 \rightarrow {}^4T_2$ transition of the octahedrally coordinated Mn^{4+} ions. Assignment of the two remaining bands is not as straightforward and requires a more careful analysis, based on the crystal field calculations. The luminescence spectrum consists of narrow lines at about 650–660 nm (~15,100–15,300 cm^{-1}), which are due to the ^2E, $^2T_1 \rightarrow {}^4A_2$ spin-forbidden transitions.

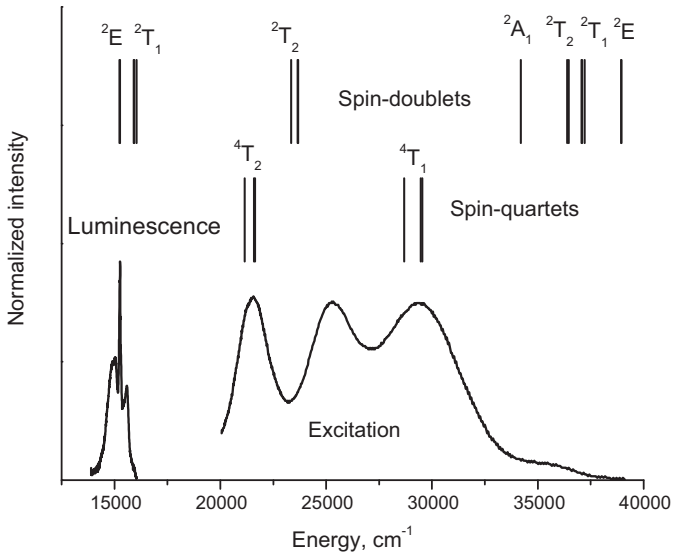

Fig. 5. Excitation and luminescence room temperature spectra of $CaAl_{12}O_{19}$:Mn^{4+} (solid line) and calculated energy levels of Mn^{4+} (vertical lines).

Crystal field theory can be successfully applied for analysis and assignment of the main features of the absorption/excitation spectra of impurity ions in crystals. It is based on representation of the crystal field Hamiltonian in the form of linear combination of operators O_p^k (which are combinations of spherical operators), which in the case of 3d ions is

$$H = \sum_{p=2,4} \sum_{k=-p}^{p} B_p^k O_p^k \quad (1)$$

(for rare earth ions the terms with $p = 6$ should be added). The B_p^k entries are the crystal field parameters (CFPs), which can be calculated directly from the crystal structure data. The exchange charge model (ECM) of crystal field [21] has been used to calculate the CFPs in the considered system. The main advantage of this model is that it allows for direct taking into account effects of overlap between the wave functions of the central ion and ligand, which lead to the formation of the covalent bond between interacting ions. Explicit expressions for calculations of the crystal field parameters in this model are as follows [21]:

$$B_p^k = B_{p,q}^k + B_{p,S}^k, \quad (2)$$

where

$$B_{p,q}^k = -K_p^k e^2 \left\langle r^p \right\rangle \sum_i q_i \frac{V_p^k(\theta_i, \varphi_i)}{R_i^{p+1}} \quad (3)$$

$$B_{p,S}^k = K_p^k e^2 \frac{2(2p+1)}{5} \sum_i (G_s S(s)_i^2 + G_\sigma S(\sigma)_i^2 + \gamma_p G_\pi S(\pi)_i^2) \frac{V_p^k(\theta_i, \varphi_i)}{R_i} \quad (4)$$

The first term $B_{p,q}^k$ is the point charge contribution to the CFPs, which effectively describes electrostatic interaction between the central ion and the crystal lattice ions denoted by index i with charges q_i and spherical coordinates, R_i, θ_i, φ_i (in the reference system centered at the impurity ion itself). The $\left\langle r^p \right\rangle$ values are the moments of the electron density distribution, which can be calculated numerically, provided that the radial parts of the corresponding wave functions are known. The values of the numerical factors K_p^k, γ_p, the expressions for the polynomials V_p^k and the definitions of the operators O_p^k can all be found in Ref. [21] and thus are not shown here for the sake of brevity.

Table 1
Non-zero CFPs values (all in cm^{-1}; Stevens normalization) for Mn^{4+} ions in $CaAl_{12}O_{19}$. ECM fitting parameter $G = 5.85$.

Parameter	$CaAl_{12}O_{19}$		
	$B_{p,q}^k$	$B_{p,S}^k$	Total value
B_2^{-2}	−188.9	0	−188.9
B_2^{-1}	−4.1	0	−4.1
B_2^0	−1394.3	1220.5	−173.8
B_2^1	−3.2	0	−3.2
B_2^2	109.4	0	109.4
B_4^0	−551.9	−3450.0	−4001.9
B_4^3	14,874.9	89,034.5	103,909.4

The second term $B_{p,S}^k$ given by Eq. (4) improves considerably the point charge model of crystal field. $B_{p,S}^k$ is proportional to the overlap between the wave functions of the central ion and ligands (here it is even possible to distinguish between different s-, p-, and d-states, which obviously produce different contributions into the overlap effects due to differences in the spatial distribution of electron densities) and includes into consideration all covalent effects. $S(s)$, $S(\sigma)$, and $S(\pi)$ in Eq. (4) correspond to the overlap integrals between the d-functions of the central ion and p-, s-functions of ligands: $S(s) = \left\langle d0 \middle| s0 \right\rangle$, $S(\sigma) = \left\langle d0 \middle| p0 \right\rangle$, $S(\pi) = \left\langle d1 \middle| p1 \right\rangle$ (here the $\left\langle lm \right|$ notation is used here, where l and m are the orbital and magnetic quantum numbers, respectively). The G_s, G_σ, and G_π entries are the dimensionless adjustable parameters of the ECM, whose values are determined from the positions of the first three absorption bands in the experimental spectrum by a direct matching the calculated energy levels to those deduced from the experimental spectra. It is possible very often (especially in the case of 3d ions) to use a single value, i.e. $G_s = G_\sigma = G_\pi = G$, which then can be estimated from one absorption band only. This is usually a reasonable approximation [21].

The Mn^{4+}–O^{2-} overlap integrals needed for calculations of the crystal field parameters were evaluated numerically with the help of the wave functions from Refs. [22,23]. A large cluster consisting of more than 58,600 ions was generated using the crystal structure data from Ref. [20]; such a cluster ensures convergence of the crystal lattice sums (especially for the second rank CFPs, which depend on distance R as $1/R^3$) in Eq. (3). Whereas a large cluster is considered for calculations of the point charge contributions to the CFPs (Eq. (3)), only the nearest six ligands are taken into account for the exchange charge contributions (Eq. (4)).

Table 1 shows the calculated CFPs values, which were used for diagonalization of the crystal field Hamiltonian from Eq. (1) in the basis set spanned by the wave functions of all LS terms of Mn^{4+} ion. Both contributions to the CFPs values (Eqs. (3) and (4)) are given separately. It is seen that the exchange charge contributions are very large and thus are very important for getting reliable picture of the Mn^{4+} energy levels. The structure of the CF Hamiltonian suggests trigonal symmetry of the Mn^{4+} position; only the B_2^0, B_4^0, and B_4^3 parameters are not zero, if the nearest environment of Mn^{4+} ions is considered, which is a typical form of the CF Hamiltonian for trigonal field. Non-zero values of the B_2^{-2}, B_2^{-1}, B_2^1, and B_2^2 CFPs, also listed in Table 1, come from ions from the second and further located coordination spheres, because arrangement of ions in a large cluster does not always have the same symmetry as the nearest environment of an impurity ion.

The calculated energy levels (in the energy region up to ~40,000 cm^{-1}) are presented in Table 2. It is possible to conclude that the band at 340 nm (~29,400 cm^{-1}) is due to the spin-allowed $^4A_2 \rightarrow {}^4T_1$ (^4F) transition of Mn^{4+}. Another band at 394 nm

Table 2
Positions of calculated energy levels of Mn^{4+} ions in $CaAl_{12}O_{19}$ (Racah parameters $B = 750\,cm^{-1}$, $C = 3245\,cm^{-1}$).

Energy levels (O_h group irreps.)	Calculated	Experimental
$^4A_2$	0	0
^2E	15,241, 15,259	15,243
$^2T_1$	15,905, 15,928, 16,042	15,570, 15,845
$^2T_2$	23,350, 23,653, 23,681	
$^4T_2$	21,154, 21,590, 21,636	21,460
$^4T_1$	28,692, 29,470, 29,548	29,450
$^2A_1$	34,197	
$^2T_2$	36,388, 36,460, 36,463	
$^2T_1$	37,074, 37,090, 37,217	

($\sim$25,400 cm^{-1}) can be formed by the spin-forbidden $^4A_2 \rightarrow {}^2T_2$ transition, which gains its intensity from the allowed transitions through the spin–orbit and electron–vibrational interaction. One more Mn^{4+} spin-allowed transition $^4A_2 \rightarrow {}^4T_1$ (^4P) is located at about 46,000 cm^{-1} and is out of the spectral range studied in the present work.

Comparison of the calculated energy levels of Mn^{4+} in $CaAl_{12}O_{19}$ with experimental data (Fig. 5 and Table 2) suggests reasonable agreement between both experimental and calculated energy level sets, thus voting for reliability of the performed analysis.

It is also possible now to explain a considerable red shift of the Mn^{4+} luminescence, which takes place: the brightest peak of the ^2E, $^2T_2 \rightarrow {}^4A_2$ transition shifts from 15,240 cm^{-1} to 14,750 cm^{-1} (Fig. 3).

It is well known (based on the Tanabe–Sugano diagram for the d^3-configuration, Fig. 2, inset) that position of the ^2E level is almost independent of the crystal field strength. Then the only explanation of the red shift of Mn^{4+} luminescence can be related to a decrease of the Racah parameters (in other words, enhancement of nephelauxetic effect) with lowering down the ^2E level. Such an explanation is consistent with previously reported experimental data on spectroscopy of Al_2O_3:Mn^{4+} [24]. The following values of the Racah parameters for this system were determined (in cm^{-1}): $B = 700$, $C = 3150$ [24]. Both these parameters are lower than those established for Mn^{4+} in $CaAl_{12}O_{19}$ (Table 2), in agreement with proposed explanation. This indeed shows that considerable change of interaction of Mn^{4+} ions with environment occurs when Mg ions are added into $CaAl_{12}O_{19}$ and two separate phases Al_2O_3 and $MgAl_2O_4$ are formed.

We also note here that when two crystalline phases coexist in one sample, orientation of these crystallites can be quite random, which would produce some additional stresses and may result in existence of more than one luminescent center.

The presence of Mg^{2+} ions somewhere in the second coordination sphere around emitting Mn^{4+} ions would not affect significantly the CFPs values (which depend on the distance R as $1/R^3$ and $1/R^5$ for the second and fourth rank CFPs, respectively), especially taking into account quite different magnitudes of the second and fourth rank CFPs (Table 1). So our crystal field analysis—although it has been performed for pure $CaAl_{12}O_{19}$—remains valid for $CaAl_{12}O_{19}$ with addition of MgO as well.

It should be also mentioned here that distribution of these phases in the prepared samples is hard to be identified and controlled precisely. Therefore, quantitative analysis of the prepared phosphors, in which $CaAl_{12}O_{19}$ is mixed up with MgO and doped with Mn^{4+} ions, represents an extremely difficult task. The resultant emission spectra represent a superposition of luminescence spectra from (presumably) several different Mn^{4+}-related centers in the Al_2O_3 domains, surrounded (and thus affected) by the $MgAl_2O_4$ domains. However, even in spite of such a complicated picture of formation of emitting centers in this mixed phosphor ($CaAl_{12}O_{19}$, MgO):Mn^{4+}, the studied material and its emission properties reveal high potential for future applications.

5. Conclusions

A red phosphor CAO:Mn has been synthesized and its photoluminescence properties have been studied. A strong absorption in blue region and a pure red emission make it attractive as a conversion phosphor for YAG:Ce associated white LEDs with high color rendering index. Mixing with MgO has brought a significant increase of the photoluminescence of CAO:Mn by incorporation of Mg^{2+} to the lattice. Two new phases Al_2O_3 and $MgAl_2O_4$ induced by MgO addition also reduce concentration quenching effect of Mn^{4+} in CAO. Mixing MgO into CAO:Mn with relatively higher concentration of Mn^{4+} is preferred to gain the maximum of luminescent efficiency since high concentration of luminescent centers but low cross energy transfer rate is favorable. Application of the exchange charge model of crystal field allows for calculating the values of the crystal field parameters acting upon Mn^{4+} electrons and its energy levels, which are in reasonable agreement with experimental spectra. A tentative explanation of the red shift of Mn^{4+} luminescence with addition of Mg ions was proposed, based on decrease of the Racah parameters and enhancement of the nephelauxetic effect when Mn^{4+} ions enter Al_2O_3 phase formed after incorporation of Mg ions.

Acknowledgements

Work performed at Argonne National Laboratory was supported by the U.S. Department of Energy, Office of Basic Energy Sciences, Division of Chemical Sciences, Geosciences, and Biosciences, under contract DE-AC02-06CH11357. M.G. Brik thanks Estonian Science Foundation (Grants Nos. 7456, JD69, 6999 and 6660).

References

[1] M. Yamada, T. Naitou, K. Izuno, H. Tamaki, Y. Murazaki, M. Kameshima, T. Mukai, Jpn. J. Appl. Phys. 42 (2003) L20.
[2] R. Mueller-Mach, G.O. Mueller, M.R. Krames, IEEE J. Sel. Topics Quantum Electron 8 (2002) 339.
[3] R.J. Xie, N. Hirosaki, M. Mitomo, K. Takahashi, K. Sakuma, Appl. Phys. Lett. 88 (2006) 101104.
[4] C.C. Chiang, M.S. Tsai, M.H. Hon, J. Electrochem. Soc. 155 (2007) J326.
[5] M. Kottaisamy, P. Thiyagarajan, J. Mishra, M.S.R. Rao, Mater. Res. Bull. 43 (2008) 1657.
[6] K. Zhan, H.Z. Liu, Y.T. Wu, W.B. Hu, J. Mater. Sci. 42 (2007) 9200.
[7] Y.X. Pan, M.M. Wu, Q. Su, J. Phys. Chem. Solids 65 (2004) 845.
[8] H. Ryu, B.K. Singh, K.S. Bartwal, M.G. Brik, I.V. Kityk, Acta Mater. 56 (2008) 358.
[9] W.M. Yen, S. Shionoya, H. Yamamoto, Phosphor Handbook, CRC Press, 2006.
[10] W.M. Yen, S. Shionoya, H. Yamamoto, Practical Applications of Phosphors, CRC Press, 2006.
[11] G. Kemeny, C.H. Haake, J. Chem. Phys. 33 (1960) 783.
[12] A. Bergstein, W.B. White, J. Electrochem. Soc. 118 (1971) 1166.
[13] T. Murata, T. Tanoue, M. Iwasaki, K. Morinaga, T. Hase, J. Lumin. 114 (2005) 207.
[14] Y.X. Pan, G.K. Liu, Opt. Lett. 33 (2008) 1816.
[15] A. Jouini, A. Yoshikawa, A. Brenier, T. Fukuda, G. Boulon, Phys. Stat. Sol. (c) 4 (2007) 1380.
[16] V. Singh, R.P.S. Chakradhar, J.L. Rao, D.K. Kim, J. Solid State Chem. 180 (2007) 2067.
[17] J.P. Ziel, J. Chem. Phys. 57 (1972) 2442.
[18] G.F. Imbusch, Phys. Rev. 153 (1967) 326.
[19] A.L. Schawlow, D.L. Wood, A.M. Clogston, Phys. Rev. Lett. 3 (1959) 271.
[20] A. Utsunomiya, K. Tanaka, H. Morikawa, F. Marumo, H. Kojima, J. Solid State Chem. 75 (1998) 197.
[21] B.Z. Malkin, in: A.A. Kaplyanskii, B.M. Macfarlane (Eds.), Spectroscopy of Solids Containing Rare-Earth Ions, North-Holland, Amsterdam, 1987, pp. 33–50.
[22] E. Clementi, C. Roetti, Atom Data Nucleic Data Tables 14 (1974) 177.
[23] M.V. Eremin, Spectroscopy of Crystals, Nauka, Leningrad, 1989, pp. 30–44 (in Russian).
[24] E. Feher, M.D. Sturge, Phys. Rev. 172 (1968) 244.